ANALYSIS OF ANTIPROTON REACTIONS AT 100 GeV/c

Cambridge, Fermilab, Michigan State

Collaboration

Presented by W. W. Neale

To appear in the Proceedings
of the 1975 International
Conference on High Energy Physics
held at Palermo. Italy.

ANALYSIS OF ANTIPROTON REACTIONS AT 100 GeV/c

Cambridge, Fermilab, Michigan State Collaboration

Presented by W. W. Neale.

1. INTRODUCTION

We present preliminary results from a 98,000 picture exposure of the Fermilab 30-inch bubble chamber to a 100 GeV/c particle beam enriched with antiprotons [1]. One half of the observed interactions in the bubble chamber are due to antiprotons the remainder being due to negative pions. The downstream wide gap spark chambers and upstream tagging system were used in this experiment.

In particular we shall discuss data we have obtained on

i) Topological Cross Section.
ii) Elastic Scattering.
iii) Strange Particle Production.
iv) Inclusive pion production.

comparison with other data will be made where relevant.

Since the bubble chamber run was completed only at the end of January 1975 and the results have only become available in presentable form during the last few days we must of necessity restrict ourselves to a description of the data with little theoretical comment.

2. TOPOLOGICAL CROSS SECTIONS

Based on a sample of 58,000 pictures of which about one fifth was double scanned the topological cross sections given in Table 1 were obtained. Corrections have been made taking into account scanning efficiency, Dalitz pair productions and strange particle decays, electron pairs and secondary interactions occuring near the vertex. Our results on π^-p topological cross sections obtained at the same time agree with those of Berger et al. [2] and we feel confident that any residual systematic errors are likely to be much smaller than the statistical errors.

The values of various moments of the charged particle multiplicity distribution (excluding elastic 2 prong events) are given in Table 2 along with corresponding results from a pp exposure [3] at a similar momentum.

Our cross sections are plotted along with values obtained at lower momenta [4] in Fig.1. It can be seen that the cross sections for 8 prongs and above are still rising at 100 GeV/c. In figure 2 the variation of $\langle n \rangle$ and $\langle n \rangle / D$ is shown as a function of s, the square of the total c.m.s. energy, for $\bar{p}p$ and pp collisions [4]. The difference in the mean multiplicities seems to be constant. Over the range of s shown the value of $\langle n \rangle / D$ for the $\bar{p}p$ collisions appears fairly constant whereas there is considerable variation in pp collisions over the same range. Finally in Figure 3 the topological cross

sections at 100 GeV/c are plotted for $\bar{p}p$ and pp collisions for comparison.

It is tempting to ascribe the observed differences in the various quantities to the presence of annihilation events in $\bar{p}p$ collisions.

Table 1.

Topological Cross Section for 100 GeV/c $\bar{p}p$ Interactions

Prong Number	Raw Events	Corrected Events	Cross Section [a] (mb)
0	11	13	0.06 ± 0.02
2 Elastic	1876	1635	7.41 ± 0.38
Inelastic		794	3.60 ± 0.30
4	1664	1777	8.05 ± 0.20
6	1765	1821	8.25 ± 0.20
8	1527	1528	6.93 ± 0.18
10	937	907	4.11 ± 0.13
12	513	484	2.19 ± 0.10
14	215	199	0.90 ± 0.06
16	82	80	0.36 ± 0.04
18	26	26	0.12 ± 0.02
20	9	9	0.041 ± 0.014
22	2	2	0.009 ± 0.006
Total Inelastic	-	7640	34.63 ± 0.22
Total	8626	9275	42.04 ± 0.09 [b]

a) Errors are statistical only except for the 2 prong cross sections.

b) A. S. Carroll et al., Phys. Rev. Lett. 33 (1974) 365. The cross sections have been normalised to the measured total cross section of these authors.

Table 2

Moments of Charged Particle Multiplicity Distribution in 100 GeV/c $\bar{p}p$ Collisions

Moment	Value	102 GeV/c pp Value [a]
$\langle n \rangle$	6.74 ± 0.04	6.32 ± 0.07
$\langle n \rangle / D$	2.07 ± 0.03	2.02 ± 0.03
f_2	3.85 ± 0.18	3.45 ± 0.25

a) C.M. Bromberg et al., Phys. Rev.Lett. 31 (1973) 1563.

3. ELASTIC SCATTERING

The two prong events have been measured and fits to the elastic scattering hypothesis attempted. Assuming a simple exponential form $\frac{d\sigma}{dt} = A\, e^{bt}$ for the elastic t distribution then using our data for $|t| > 0.08$ $(GeV/c)^2$ we find $b = 11.4 \pm 0.6$ $(GeV/c)^{-2}$ and an elastic scattering cross section of $\sigma_{el} = 7.4 \pm 0.4$ mb. The intercept at $|t| = 0$ is close to the optical theorem point.

At the same time we find for $\pi^- p$ collisions an elastic scattering cross section $\sigma_{el} = 3.5 \pm 0.2$ mb and a slope parameter $b = 7.7 \pm 0.4$ $(GeV/c)^2$.

4. STRANGE PARTICLE PRODUCTION

All events with V's have been measured on about one-third of the film including obvious electron pairs. Fits were attempted to the Λ^o, $\bar{\Lambda}^o$, K^o_s and γ hypotheses and assignments made to one or other on the basis of χ^2 probability, transverse momentum of the decay products, and mass assignments based on ionization estimates. Using only those particle produced in the backward hemisphere in the centre of mass we obtain the estimates of cross sections for $\Lambda^o/\bar{\Lambda}^o$, $K^o/\bar{K}^o$ and π^o production given in Table 3.

These results are plotted along with lower momentum $\bar{p}p$ results and pp data [4] for comparison in Figs. 4-6. The $K^o/\bar{K}^o$ and π^o cross sections for $\bar{p}p$ collisions are consistently higher than the corresponding values for pp collisions. In the case of Λ^o production it should be remembered that this will depend on the number of protons taking part in the collision.

Table 3

Cross Sections for Neutral Particle Production in 100 GeV/c $\bar{p}p$ Collisions (Preliminary Data).

Particle	Cross Section (mb)
π^o	96 ± 6
K^o or $\bar{K}^o$	6.0 ± 0.6
Λ^o or $\bar{\Lambda}^o$	1.9 ± 0.2

In Figs. 7-9 the quantity $F_1(x)$ where

$$F_1(x) = \int \frac{2E}{\pi\sqrt{s}} \cdot \frac{d\sigma}{dx dp_\perp^2} \cdot dp^2$$

is plotted as a function of x for Λ^o, $K^o/\bar{K}^o$ and γ respectively. The results of Dao et al.[5] at 14.75 GeV/c are shown for comparison.

The mean values of $p_\perp$ obtained for produced $\Lambda^o/\bar{\Lambda}^o$, $K^o/\bar{K}^o$ and γ are given in Table 4.

Table 4

Mean Transverse Momenta of Neutral Particles produced in 100 GeV/c $\bar{p}p$ collisions (Preliminary Data).

Particle	$<p>$ (GeV/c)
γ	0.190 ± 0.012
$K^o/\bar{K}^o$	0.41 ± 0.03
$\Lambda^o/\bar{\Lambda}^o$	0.47 ± 0.05

5. INCLUSIVE PION PRODUCTION

All events have been measured on a sample of the film and any protons identified by ionization removed from the set of positive particles. The centre of mass rapidity distribution is shown for the remaining positive particles assuming them to be pions in Fig.10. As expected the distribution is broader than that for 14.75 GeV/c $\bar{p}p$ collisions shown in the same plot. For comparisons the rapidity distributions for π^+ produced in the backward hemisphere and π^- produced in the forward hemisphere in pp collisions at 100 GeV/c are also plotted. The $\bar{p}p$ and pp distributions agree in the fragmentation regions indicating factorisation, the excess of pions produced in $\bar{p}p$ collisions appearing in the central region.

The $p_\perp^2$ distributions for π^+ produced in $\bar{p}p$ collisions and π^- produced in pp collisions can be seen in Fig. 11 to have similar shape.

REFERENCES

1) W. W. Neale, "Enriched Particle Beams for the Bubble Chambers at the Fermilab National Accelerator Laboratory", FN-259 (1974).
2) E. L. Berger at al., Nucl. Phys. B77 (1974) 365.
3) C. M. Bromberg et al., Phys. Rev. Lett. 31 (1973) 1563.
4) J. Whitmore, Phys. Rep. Phys. Lett. 10C (1974) 273.
5) F. T. Dao et al., Phys. Lett. 51B (1974) 505.

FIGURE CAPTIONS

Fig. 1. Momentum dependence of $\bar{p}p$ topological cross sections. The curves are to guide the eye.

Fig. 2. Momentum and S dependence of (a) the average charged multiplicity <n> and (b) the quantity <n>/D where D is the dispersion of the multiplicity distribution, for $\bar{p}p$ and pp interactions. The curves are to guide the eye.

Fig. 3. Comparison of $\bar{p}p$ and pp topological cross sections at 100 GeV/c. The pp data are from Ref. 3.

Fig. 4. Momentum dependence of the cross section for Λ^o production in $\bar{p}p$ and pp collisions.

Fig. 5. Momentum dependence of the cross section for $K^o/\bar{K}^o$ production in $\bar{p}p$ and pp collisions.

Fig. 6. s dependence of the cross section for π^o production in $\bar{p}p$ and pp collisions.

Fig. 7. Plot of the quantity $F_1(x)$ as a function of x for Λ^o production in $\bar{p}p$ collisions at 100 GeV/c (our data) and at 14.75 GeV/c.

Fig. 8. Plot of the quantity $F_1(x)$ as a function of x for $K^o/\bar{K}^o$ production in $\bar{p}p$ collisions at 100 GeV/c and 14.75 GeV/c.

Fig. 9. Plot of the quantity $F_1(x)$ as a function of x for γ production in $\bar{p}p$ collisions at 100 GeV/c and 14.75 GeV/c.

Fig. 10. Centre of mass rapidity distribution for π^+ produced in $\bar{p}p$ collisions at 100 GeV/c and 14.75 GeV/c. The solid curves are for π^+ production in the

backward and π^- in the forward hemisphere in 100 GeV/c pp collisions.

Fig. 11. Plot of $1/2\ d\sigma/dp_\perp^2$ as a function of $p_\perp^2$ for π^+ production in $\bar{p}p$ collisions and π^- production in pp collisions at 100 GeV/c.

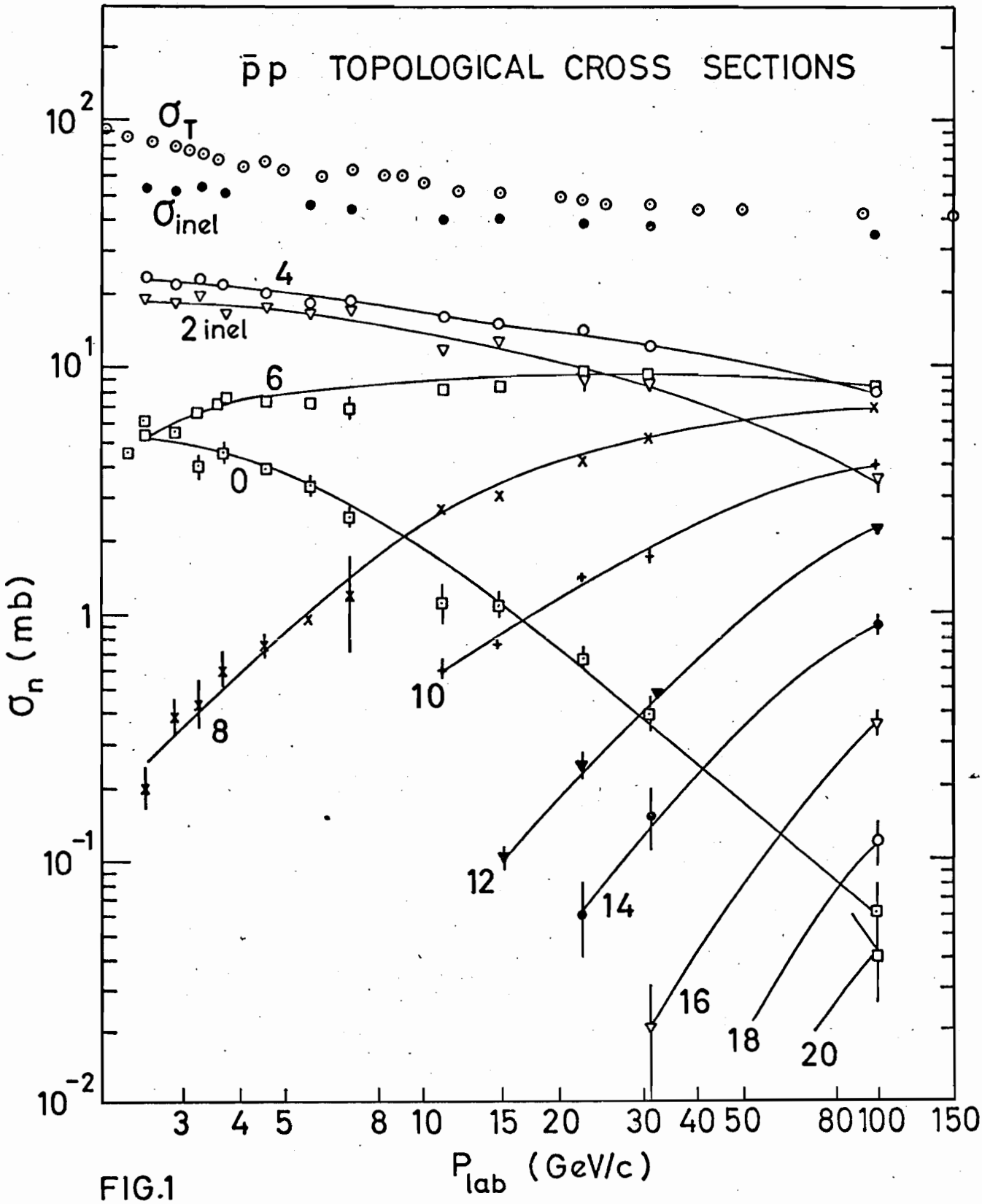
$\bar{p}p$ TOPOLOGICAL CROSS SECTIONS
σ_T
σ_{inel}
4
2 inel
6
0
8
10
12
14
16
18
20
σ_n (mb)
10^2
10^1
1
10^{-1}
10^{-2}
3 4 5 8 10 15 20 30 40 50 80 100 150
P_{lab} (GeV/c)

FIG.1

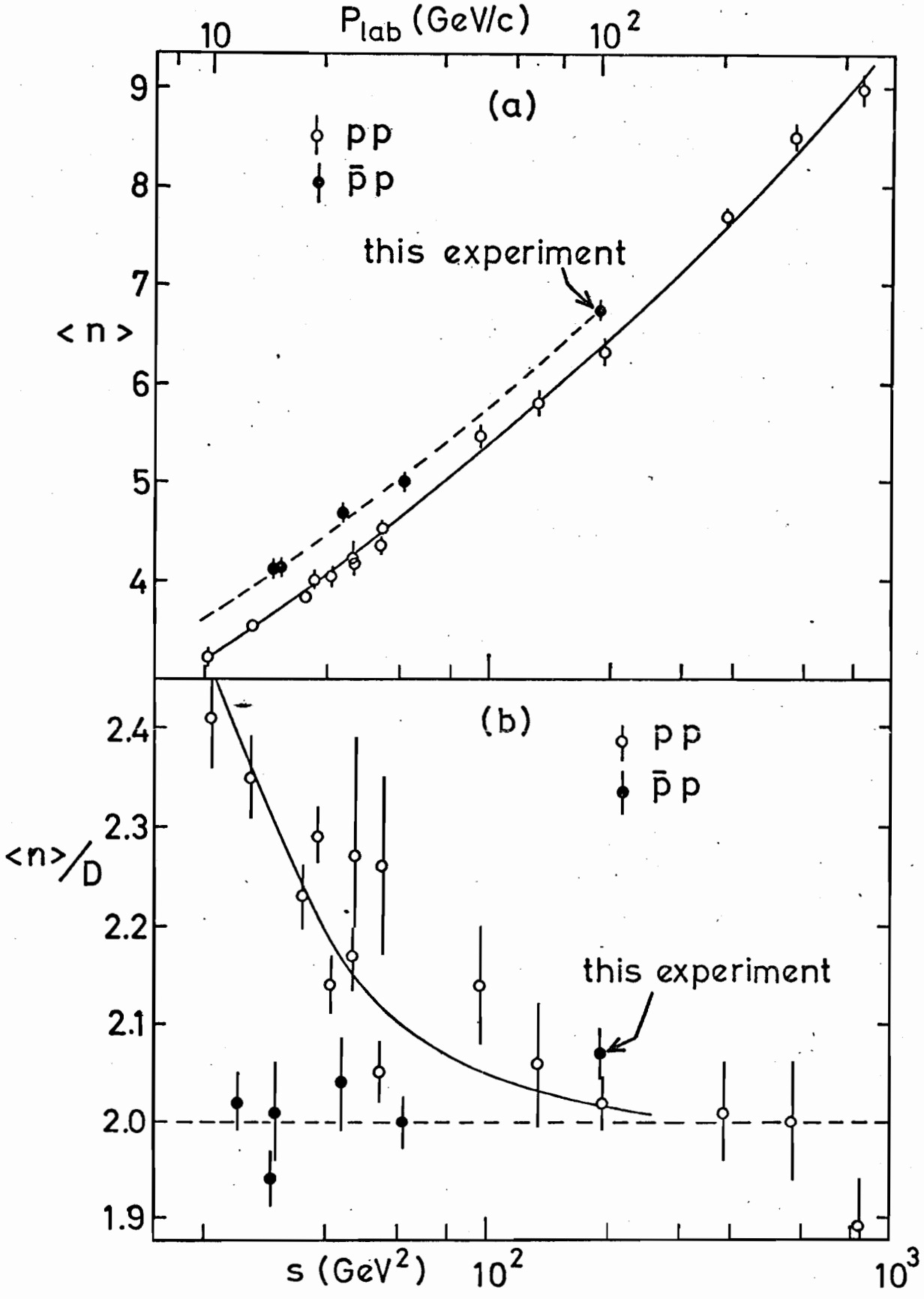
10
P_{lab} (GeV/c)
10^2
(a)
pp
$\bar{p}p$
this experiment
<n>
9
8
7
6
5
4
(b)
pp
$\bar{p}p$
this experiment
<n>/D
2.4
2.3
2.2
2.1
2.0
1.9
s (GeV^2)
10^2
10^3

FIG. 2

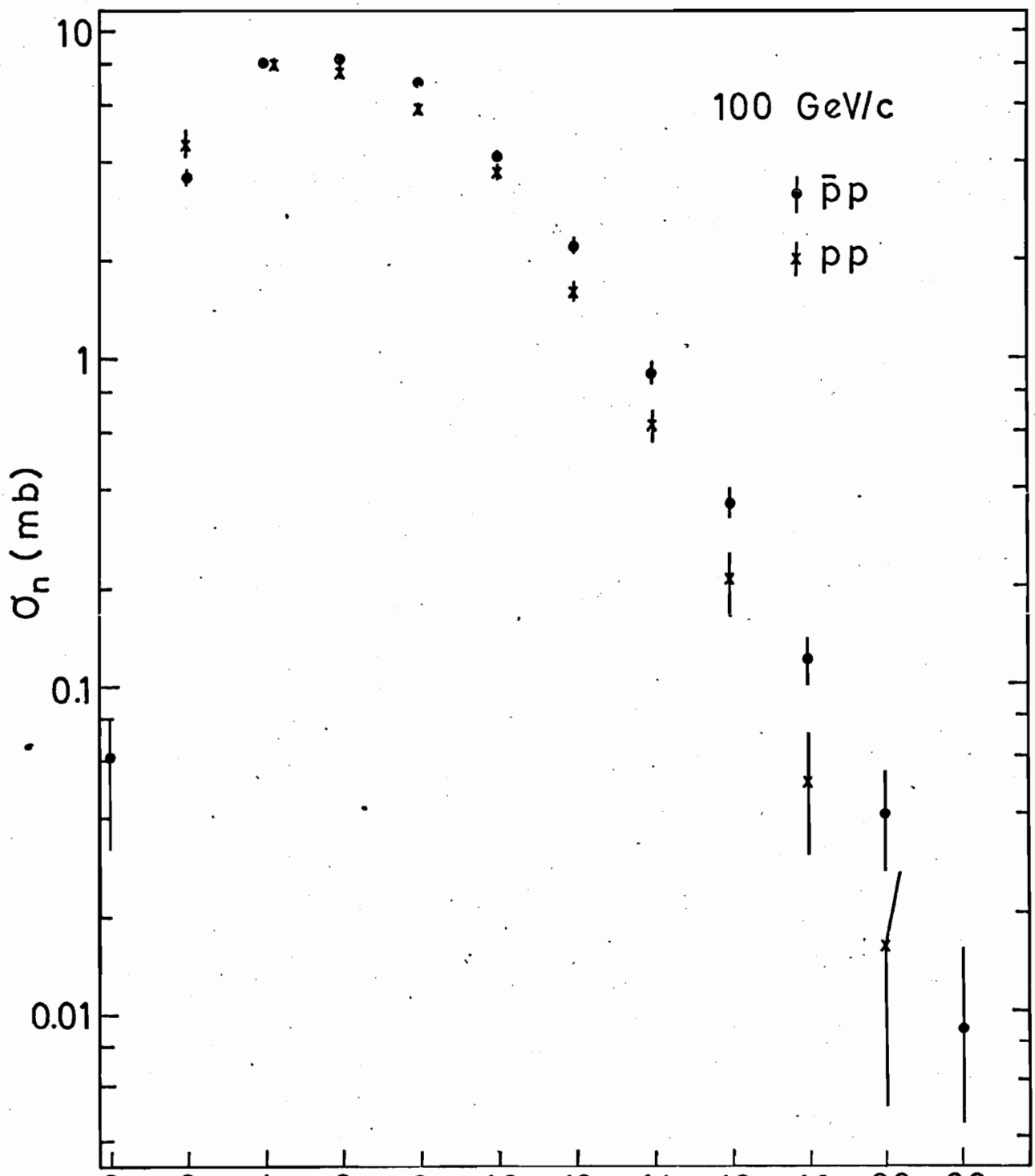

FIG.3

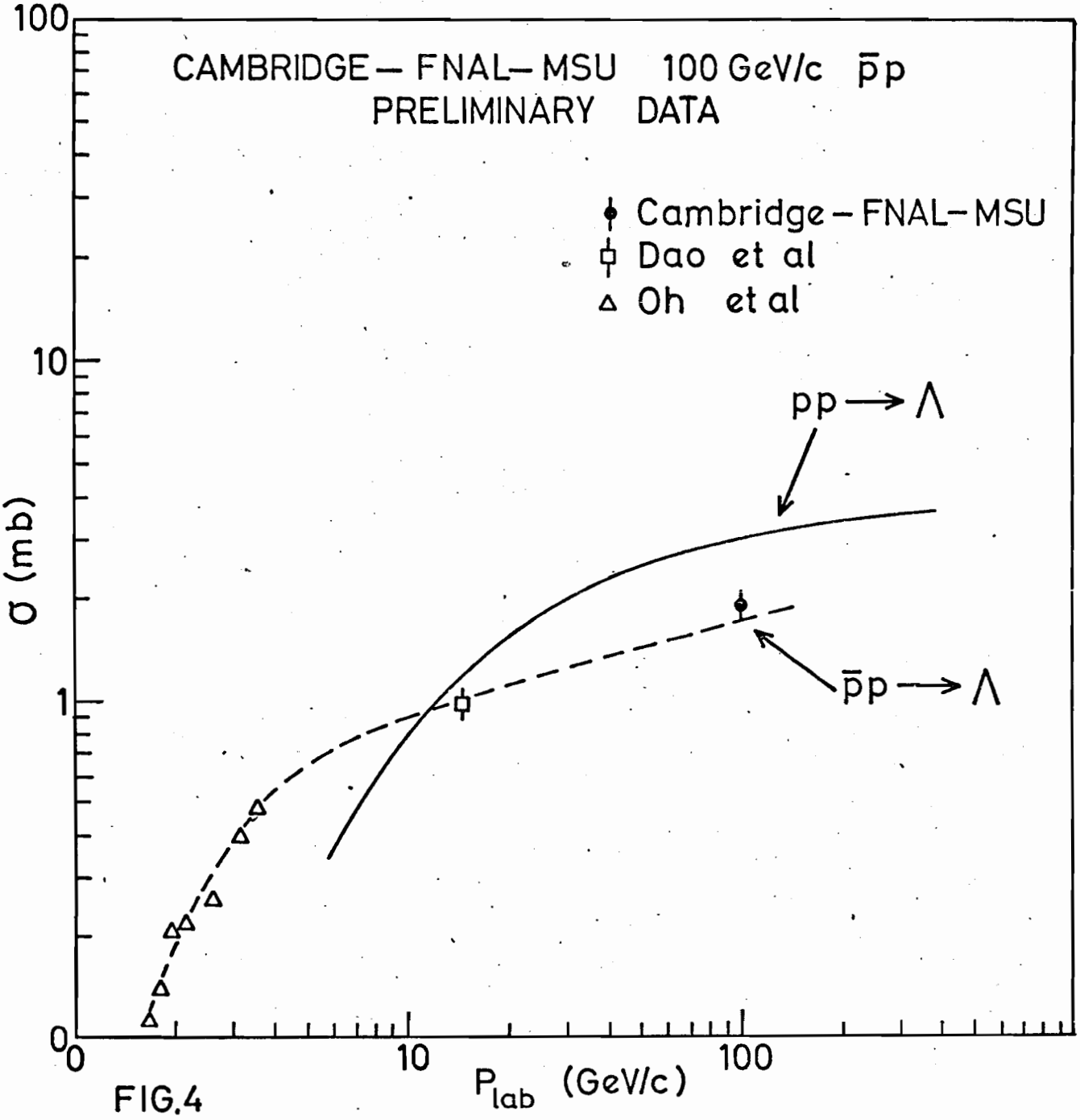
CAMBRIDGE — FNAL — MSU 100 GeV/c p̄p
PRELIMINARY DATA
Cambridge – FNAL – MSU
Dao et al
Oh et al
pp → Λ
p̄p → Λ
σ (mb)
100
10
1
0
0
10
100
P_lab (GeV/c)

FIG.4

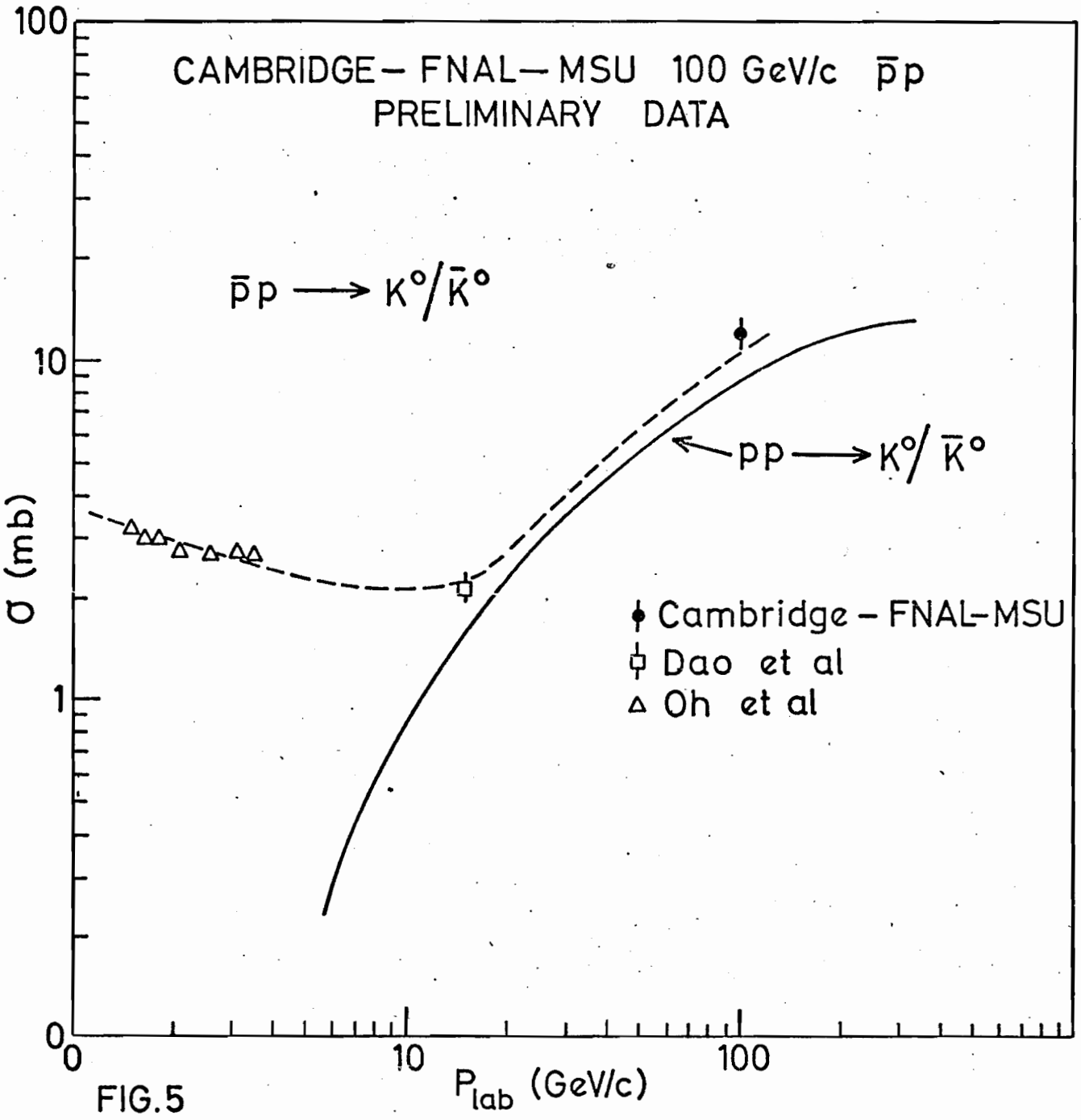
CAMBRIDGE – FNAL – MSU 100 GeV/c $\bar{p}p$
PRELIMINARY DATA
$\bar{p}p \longrightarrow K^0/\bar{K}^0$
$pp \longrightarrow K^0/\bar{K}^0$
Cambridge – FNAL–MSU
Dao et al
Oh et al
σ (mb)
100
10
1
0
0
10
100
P_{lab} (GeV/c)

FIG.5

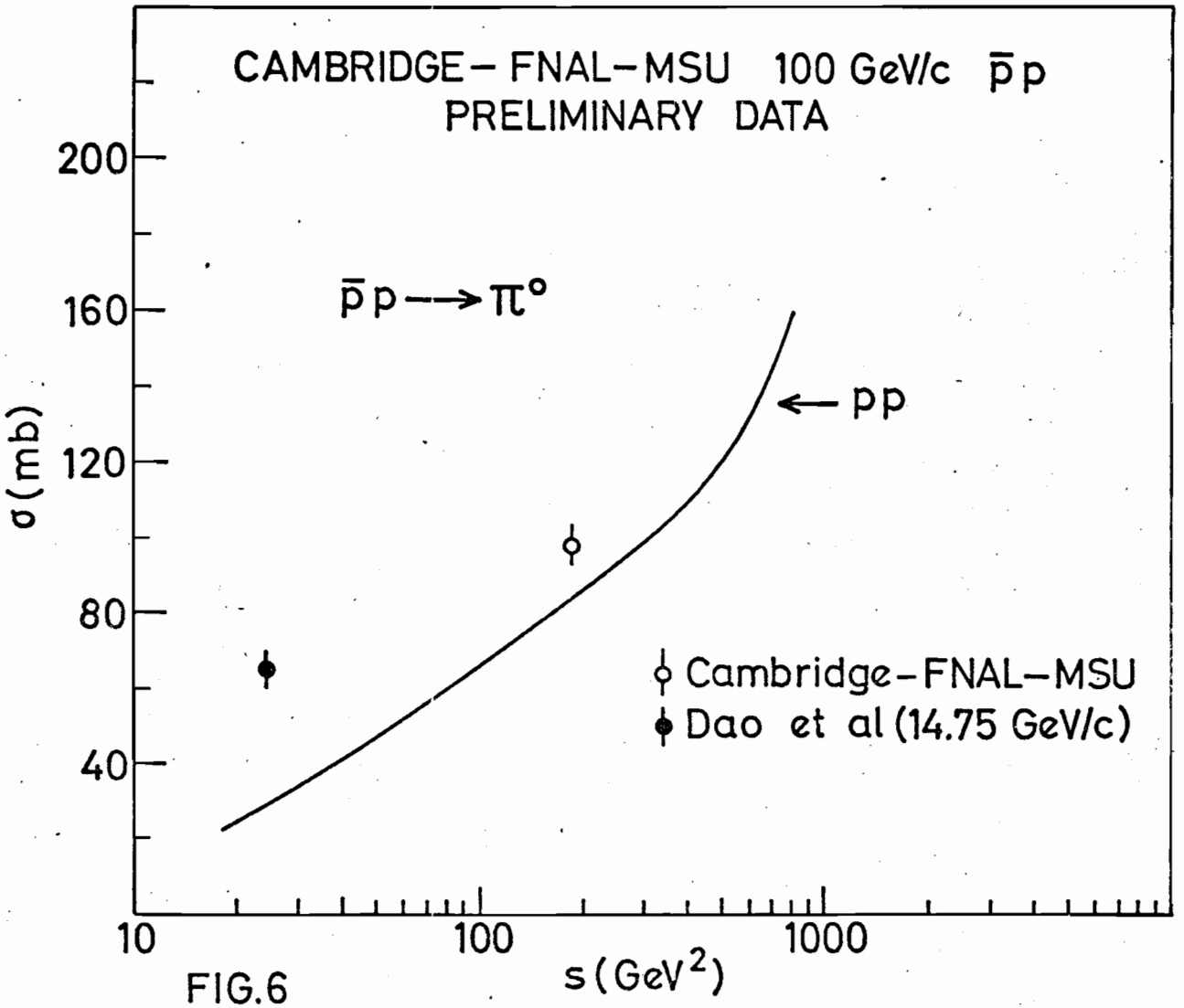
CAMBRIDGE – FNAL – MSU 100 GeV/c $\bar{p}p$
PRELIMINARY DATA
$\bar{p}p \longrightarrow \pi^0$
$\leftarrow pp$
Cambridge – FNAL – MSU
Dao et al (14.75 GeV/c)
σ (mb)
200
160
120
80
40
10
100
1000
s (GeV^2)

FIG.6

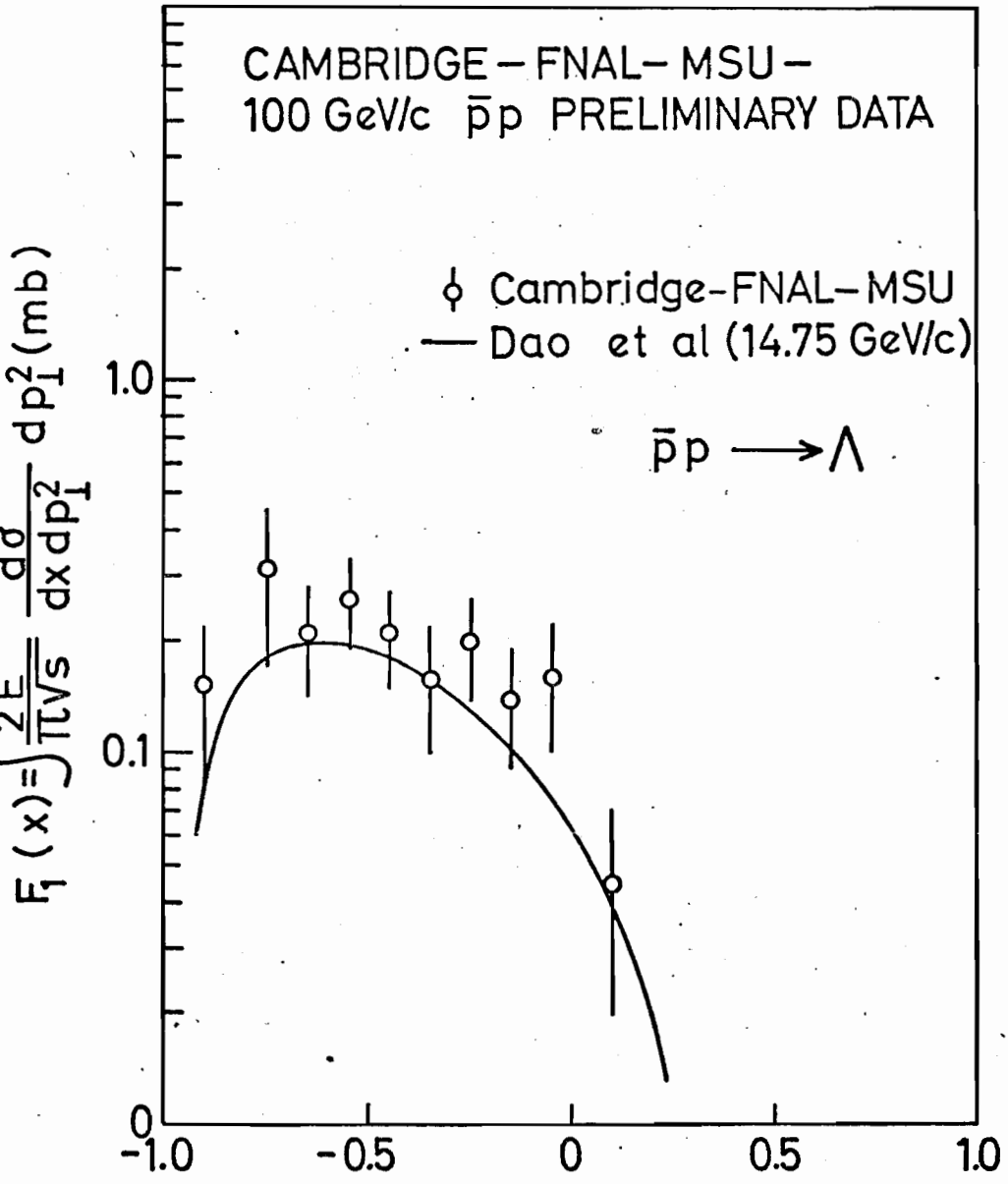
CAMBRIDGE – FNAL – MSU –
100 GeV/c p̄p PRELIMINARY DATA
Cambridge-FNAL-MSU
Dao et al (14.75 GeV/c)
p̄p ⟶ Λ
$F_1(x)=\int \frac{2E}{\pi\sqrt{s}} \frac{d\sigma}{dx\,dp_T^2} dp_T^2$ (mb)
1.0
0.1
0
-1.0
-0.5
0
0.5
1.0
x

FIG.7

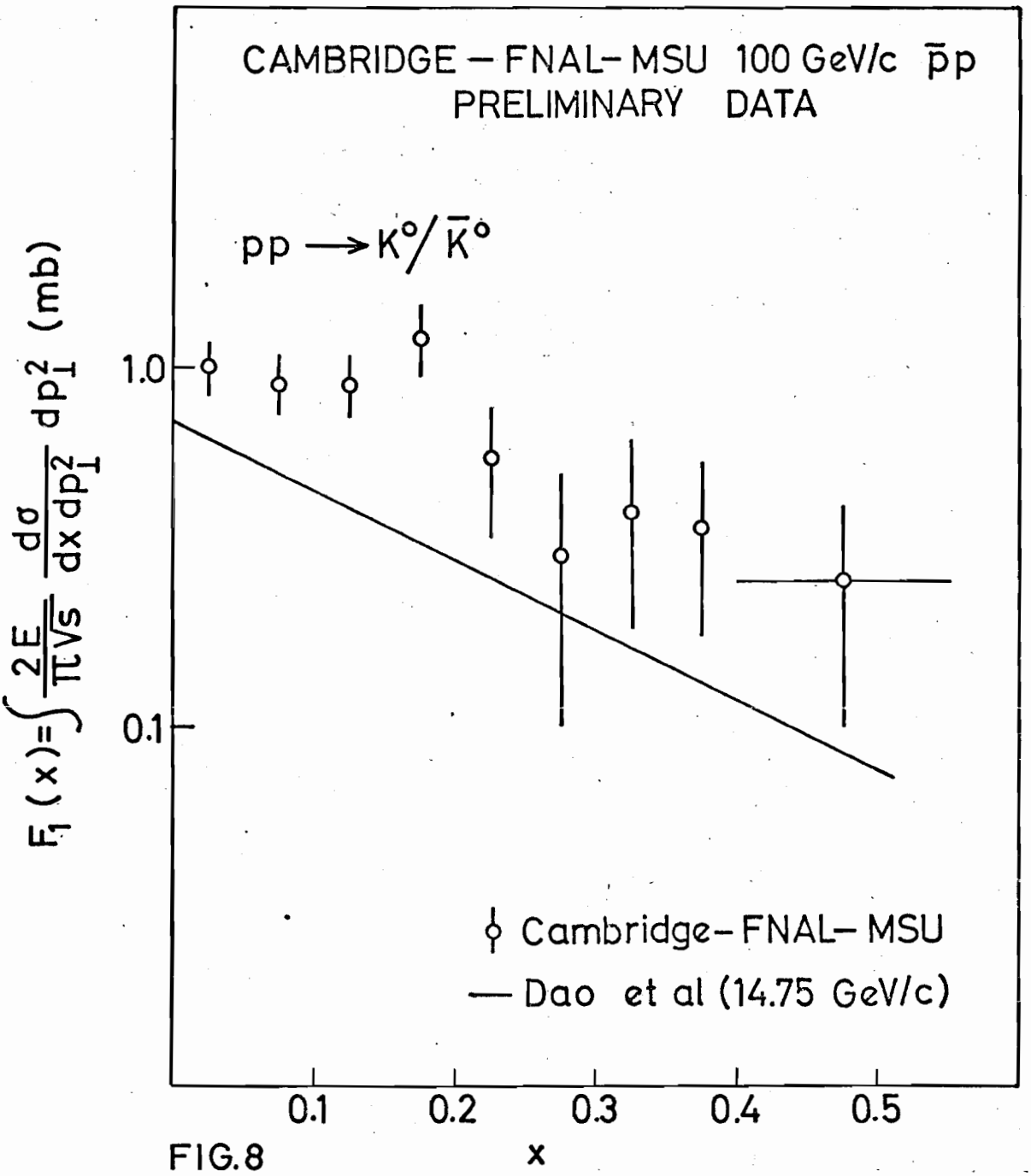
CAMBRIDGE – FNAL– MSU 100 GeV/c $\bar{p}p$
PRELIMINARY DATA
$pp \rightarrow K^0/\bar{K}^0$
$F_1(x)=\int \frac{2E}{\pi\sqrt{s}} \frac{d\sigma}{dx\,dp_T^2} dp_T^2$ (mb)
1.0
0.1
Cambridge– FNAL– MSU
Dao et al (14.75 GeV/c)
0.1
0.2
0.3
0.4
0.5
x

FIG.8

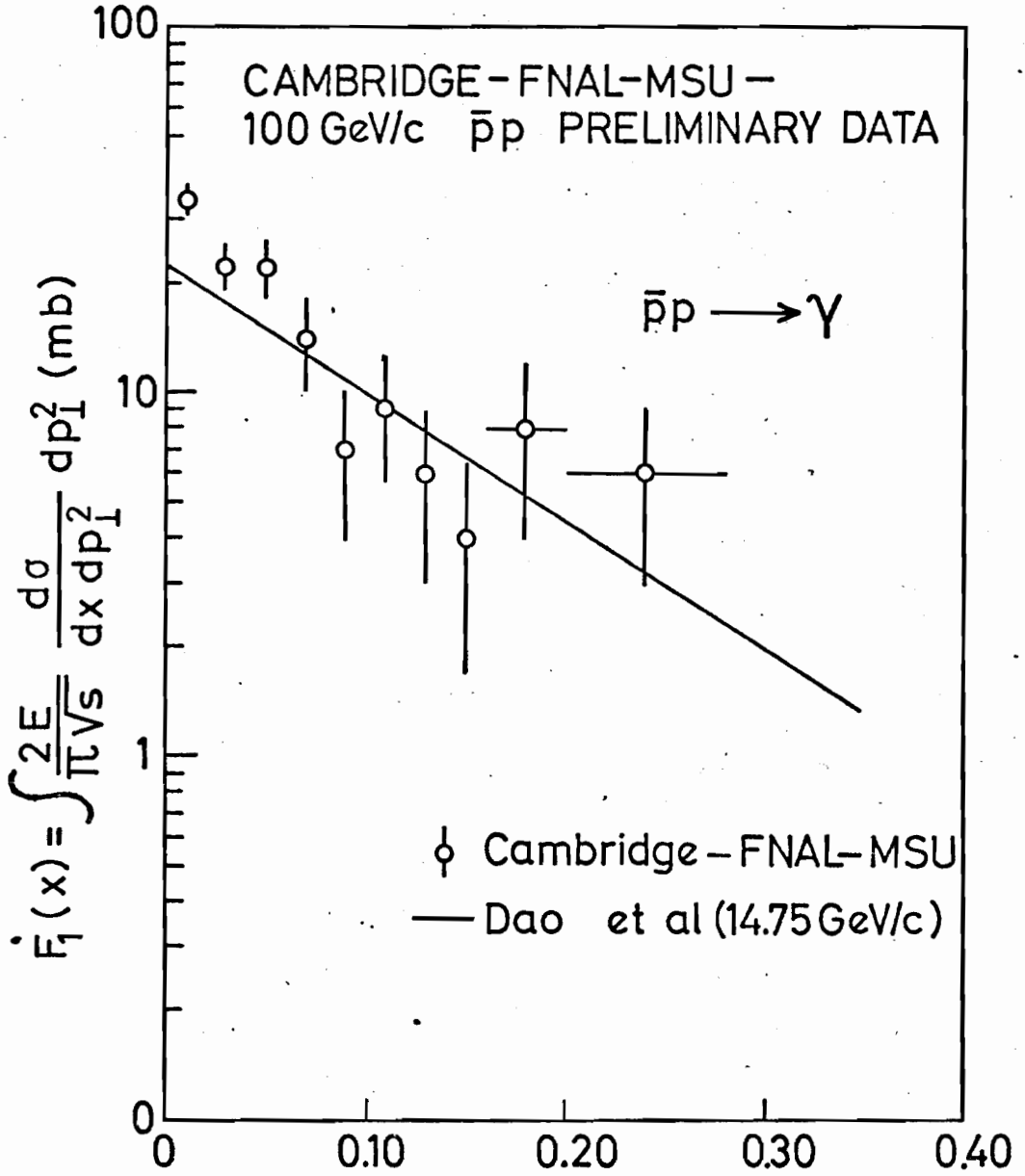
CAMBRIDGE – FNAL–MSU –
100 GeV/c p̄p PRELIMINARY DATA
p̄p → γ
Cambridge – FNAL–MSU
Dao et al (14.75 GeV/c)
$F_1(x) = \int \frac{2E}{\pi\sqrt{s}} \frac{d\sigma}{dx\, dp_T^2} dp_T^2$ (mb)
100
10
1
0
0
0.10
0.20
0.30
0.40
x

FIG.9

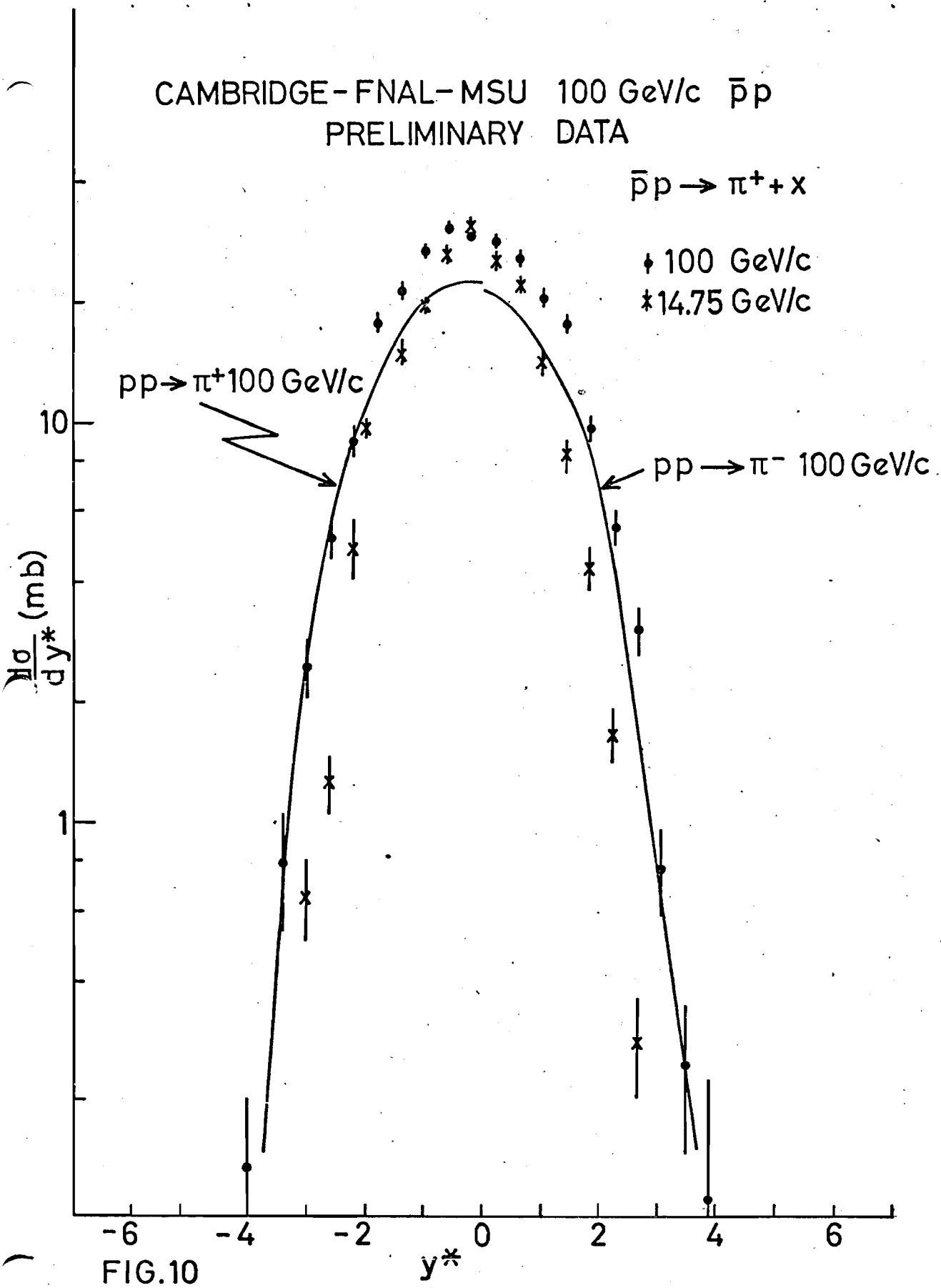
CAMBRIDGE-FNAL-MSU 100 GeV/c $\bar{p}p$
PRELIMINARY DATA
$\bar{p}p \rightarrow \pi^+ + x$
100 GeV/c
14.75 GeV/c
$pp \rightarrow \pi^+$ 100 GeV/c
$pp \rightarrow \pi^-$ 100 GeV/c
$\frac{1}{\sigma}\frac{d\sigma}{dy^*}$ (mb)
10
1
-6
-4
-2
0
2
4
6
y^*

FIG.10

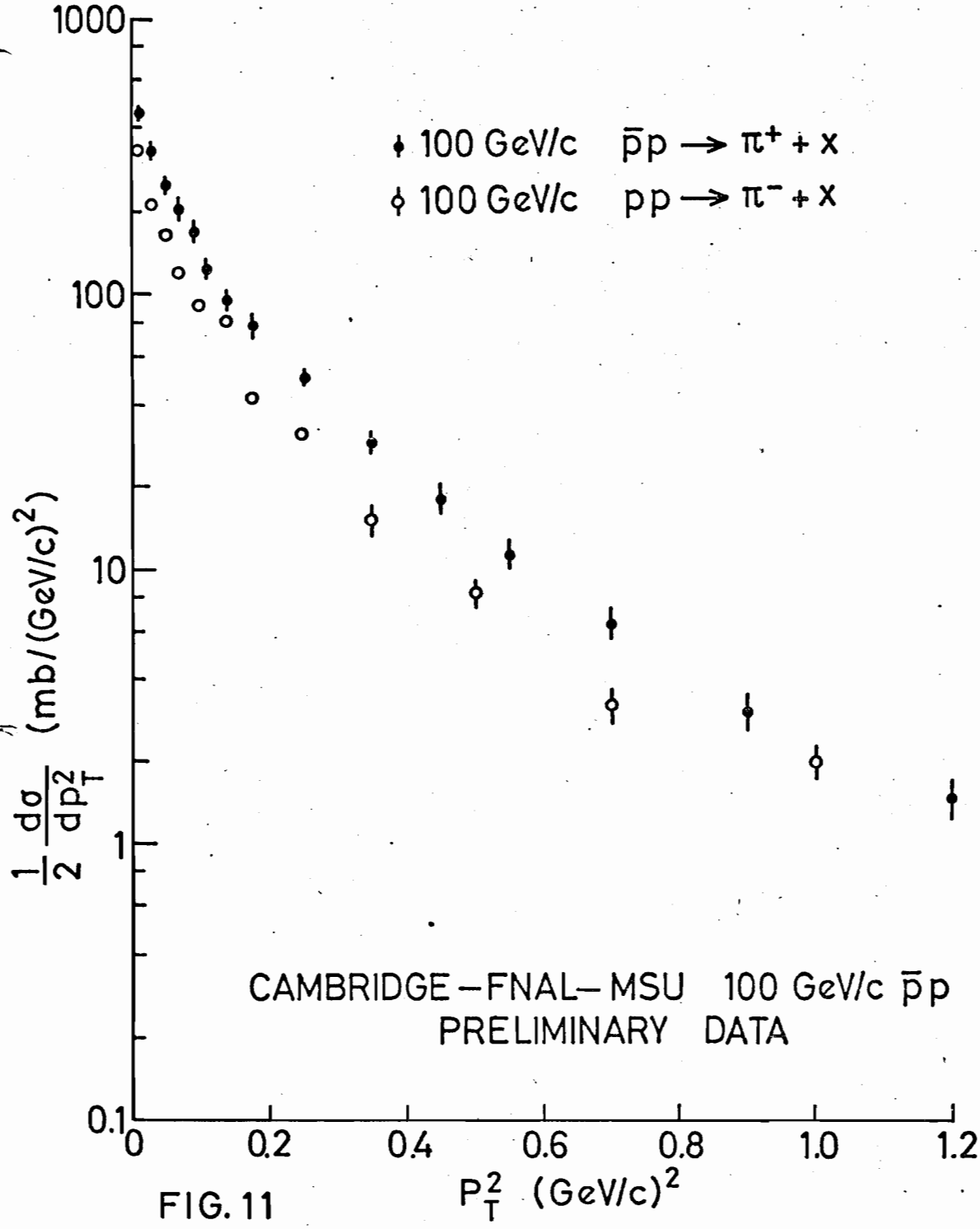
1000
100
10
1
0.1
0
0.2
0.4
0.6
0.8
1.0
1.2
100 GeV/c $\bar{p}p \rightarrow \pi^+ + x$
100 GeV/c $pp \rightarrow \pi^- + x$
$\frac{1}{2}\frac{d\sigma}{dp_T^2}$ (mb/(GeV/c)^2)
P_T^2 (GeV/c)^2
CAMBRIDGE – FNAL – MSU 100 GeV/c $\bar{p}p$
PRELIMINARY DATA

FIG. 11